CHAPTER 8

Examples and Applications
PART I: QUARTZ DEVICES

by: Hans-Joachim Wagner, Institute of Microstructure- and Information Technology (IMIT), Villingen-Schwenningen, Germany

8.I.1 Introduction and historical review [8.I.17]

Piezoelectric quartz crystal oscillators are present in almost any frequency control equipment. Under those conditions important efforts have been devoted to quartz resonators and oscillators everywhere in the world. Also demanding and important has been the development of new quartz piezoelectric sensors [8.I.17].
In this chapter, quartz resonators are presented trying to provide important concepts for new developments and applications in this field.
Resonant sensor structures with direct semidigital frequency output have been realized for several applications [8.I.1]. The exceptionally high elasticity accompanied by practically negligible hysteresis and the high chemical resistivity of the single-crystal structure make monocrystalline quartz a suitable basic material for micromechanical sensors and transducers with long-term stability [8.I.2] (see also **Fig. 8.I.1**).
When properly cut and shaped, quartz can be piezoelectrically excited to a stable mechanical resonance vibration with a high Q-value. A change of the internal energy of the quartz resonator due to mechanical deformation causes a change in the resonance frequency without the Q-value deteriorating appreciably. Therefore, assuming no sizable attenuation of the system, the frequency shift can be directly related to the deformation of the resonator, that is, the applied pressure or force [8.I.3].
A short historical review including principal milestones in piezoelectricity and quartz applications is first presented in **Table 8.I.1.**

8.I.2 Short review of the quartz micromachining technology

A commonly used fabrication process with five process steps is schematically shown in **Fig. 8.I.2** [8.I.43]. The quartz etching process step (step (5) of **Fig. 8.I.2**) is performed in an

etching apparatus for prototypes like that, schematically shown in **Fig. 8.I.3**. An etch system for production use is described in **[8.I.50]**.

Table 8.I.1 Historical review of milestones in piezoelectricity and quartz applications; based on **[8.I.17]**.

1880	Pierre and Jacques Curie	Discovery of piezoelectricity
1893	Lord Kelvin	Microscopic theory of piezoelectricity in quartz crystal
1910	Voigt	Lehrbuch der Kristallphysik
1914-18	Langevin	Work on ultrasonic detection in water
1918	Nicholson (Bell Labs)	Patent on oscillating circuit with Rochelle salt crystal (US Patent 2212845, April 10, 1918
1920	W.G. Cady	Patent on oscillating circuit with 3 vacuum tubes and quartz crystal resonator (in feedback circuit)
1921	Pierce	Pierce's first oscillator
1948	R.A. Sykes	Introduction of coated units
1952	A.W. Warner	Introduction of energy trapping (AT cut)
1972	J. Staudte	Batch processing (photolithography and chemical etching) of tuning forks
1975	E.P. Eernisse	Doubly rotated SC cuts
1975	Wilcox, Snow, Hafner and Vig	Ceramic flat pack for resonators
1976	R.J. Besson	Electrodeless BVA resonator
1987	Ueda, Kohsaka, Iino and Yamazaki	Theory to predict etching shapes in quartz crystal
1989	Watkins, Tuthill, Curlee, Koehler and Joerg	Field-assisted bonding of single crystal quartz

With suitable quartz orientation, a low undercutting rate of the masking layer can be achieved (see **Fig. 8.I.4**). Also the realization of etch shapes with steep flanks perpendicular to the z axis is possible (see **Fig. 8.I.5**). Publications giving complete three-dimensional etching diagrams are very scarce. Ueda *et al* **[8.I.43, 8.I.44]** have published on this subject (see **Fig. 8.I.6**). A great disadvantage of the material quartz in relation to the micromachined material silicon is the lack of an etchstop-technique. However, thin and smooth quartz membranes have been fabricated by Delapierre **[8.I.51]** and coworkers, see also **Fig. 8.I.7**. The work of this group is reviewed in ref. **[8.I.24]**. As in the case of

silicon, quartz can also be joined by a modified field-assisted bonding technique [8.I.46], schematically demonstrated in Fig. 8.I.8.

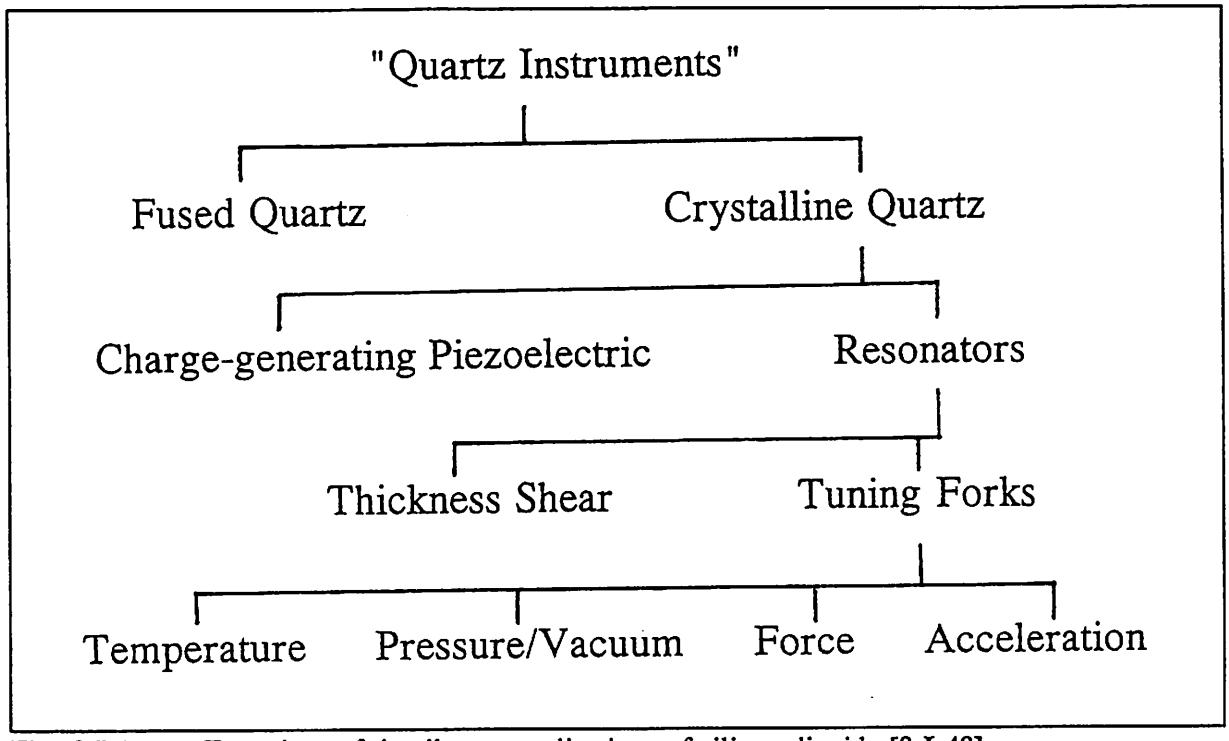

Fig. 8.I.1 Tree chart of the diverse applications of silicon dioxide [8.I.48].

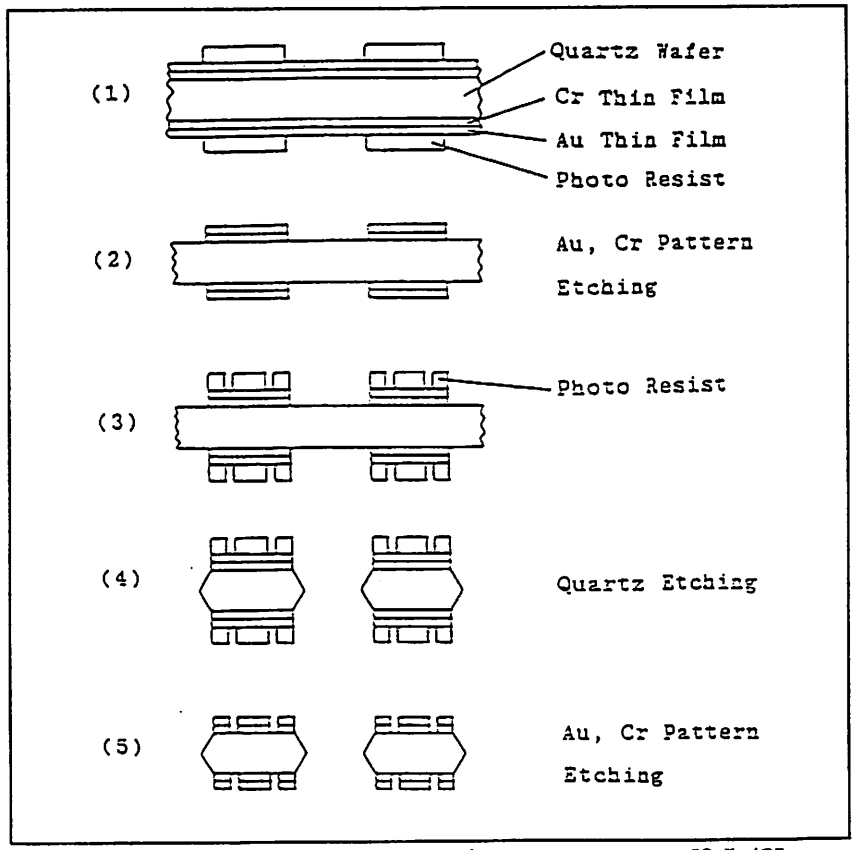

Fig. 8.I.2 Fabrication process of quartz resonator [8.I.43].

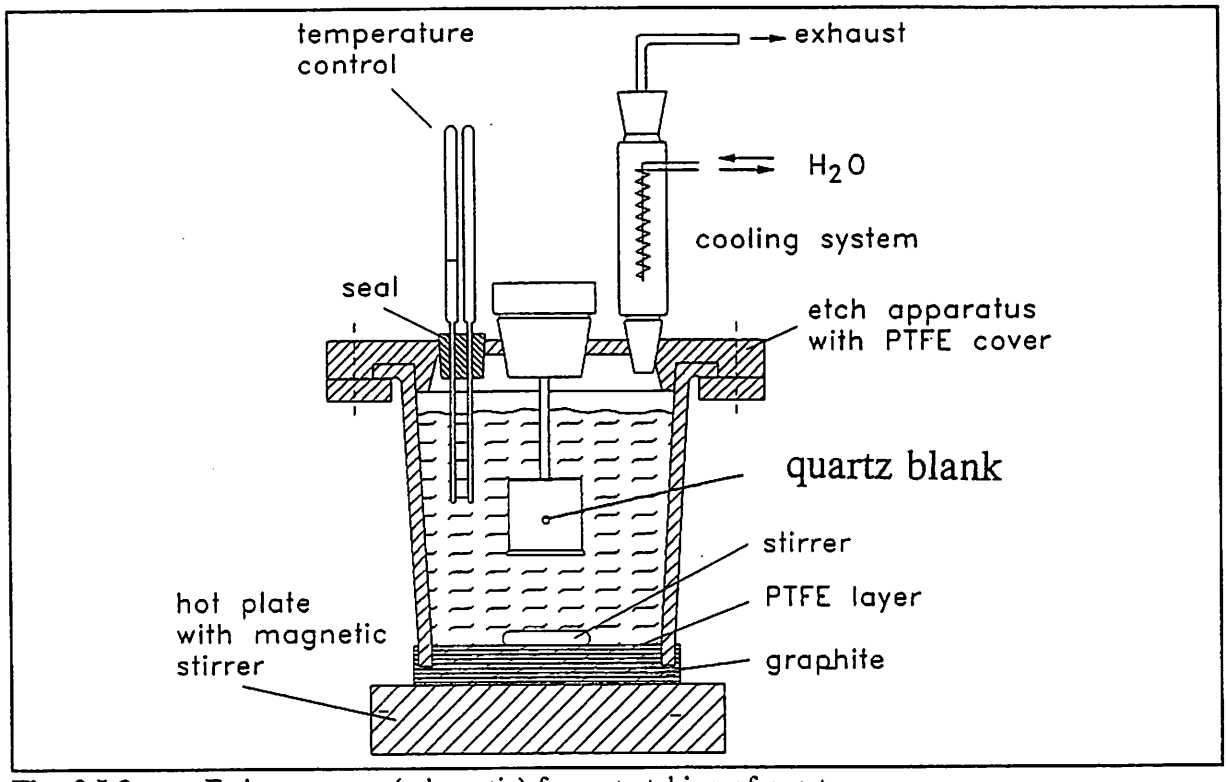

Fig. 8.I.3 Etch apparatus (schematic) for wet etching of quartz.

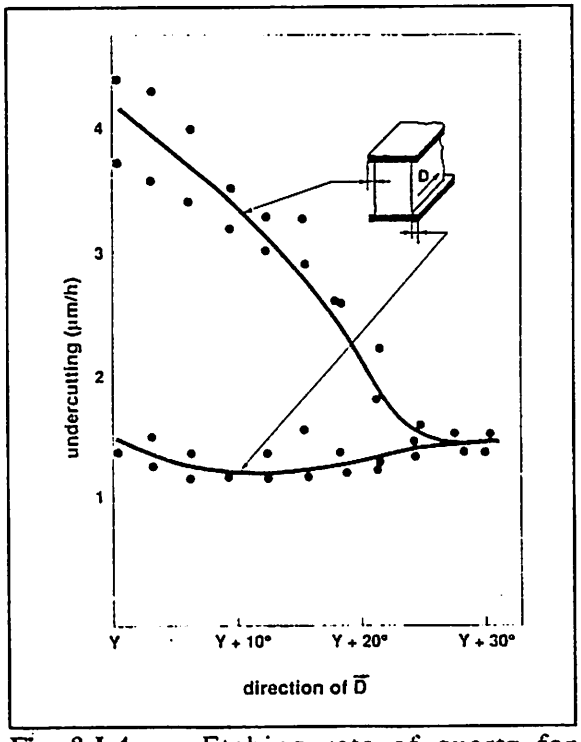

Fig. 8.I.4 Etching rate of quartz for planes parallel to the z axes [8.I.51].

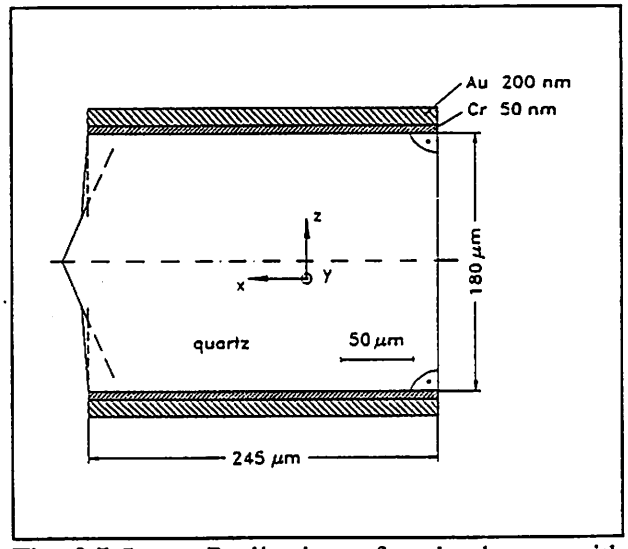

Fig. 8.I.5 Realization of etch shapes with steep flanks perpendicular to the z axis.

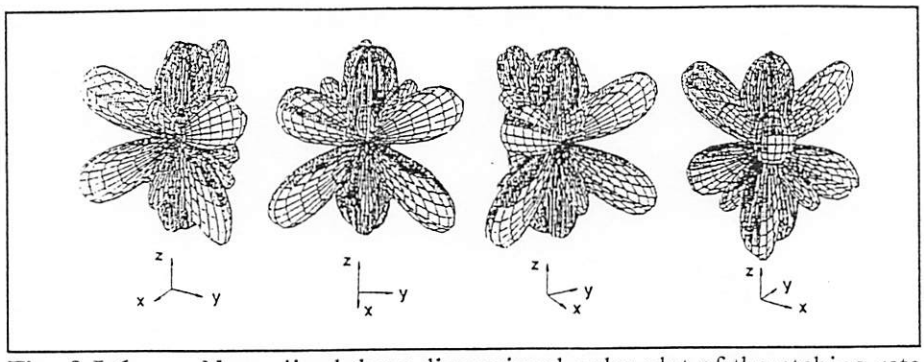

Fig. 8.I.6 Normalized three-dimensional polar plot of the etching rate of quartz in NH_4:HF_2 at 82 °C (different angle of view).

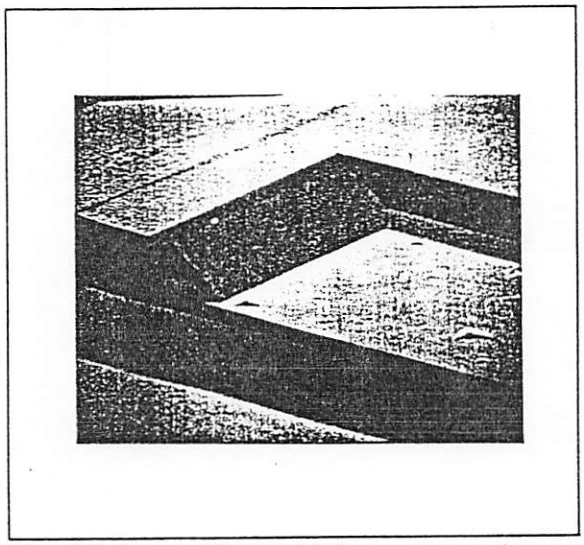

Fig. 8.I.7 30 μm thick quartz membranes in a 125 μm thick substrate [8.I.51].

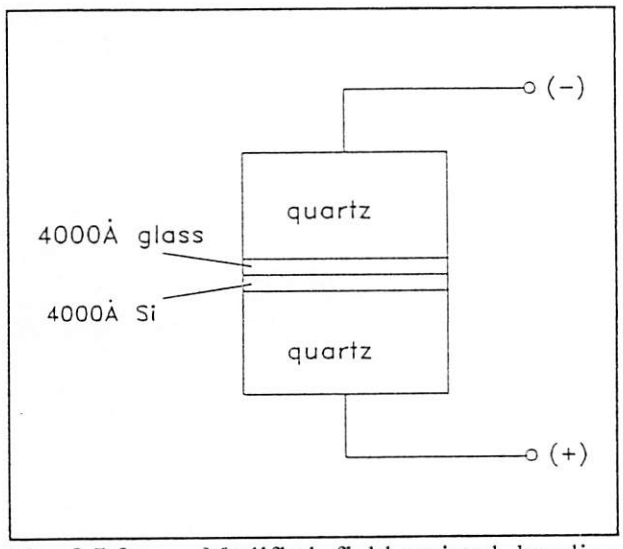

Fig. 8.I.8 Modified field-assisted bonding configuration for joining quartz to quartz [8.I.46].

8.I.3 AT-quartz pressure sensor [8.I.12]

Introduction

The resonant pressure sensor described here is based on a novel design of a quartz diaphragm realized with an AT crystal cut. The resonator consists of a full-thickness bossed diaphragm monolithically attached to the bulk frame. This design results in highly sensitive pressure sensors with low non-linearity and enhanced manufacturability [8.I.4]. The quartz diaphragm is additionally grooved in a special relation to the crystallographic axes allowing a body shear effect. Applied pressure induces a deformation of the diaphragm. Extensive finite-element modelling has been carried out to determine the electrode configuration and the shape of the structure for exciting a low- frequency bending resonance mode in the 30 - 50 kHz range. The selectivity of this vibration mode due to a barometric pressure change manifests itself as a very sensitive and stable frequency shift response of $\approx$ 7%/bar.

Principle of operation

The pressure-dependent frequency shift of a resonant diaphragm structure arises essentially

from the change of stiffness in the system. This change is achieved by structuring the quartz diaphragm of bulk thickness in such a manner that the 'knee leverage principle' can be exploited. An external pressure induces stress in the system, which is coupled with an increased amount to the hinge regions. Due to the flat leverage angle, even small deformations of the diaphragm result in a change of the resonance frequency.

Piezoelectric excitation

A quartz crystal placed in an electric field may experience a mechanical strain, which can be considered to be proportional to the applied field. This relation can be written in matrix form as

$$x = d\,E\,,$$

where x is the strain and E is the electric field (see **Table 8.I.2**). The constants d_{ij} are the piezoelectric strain coefficients. Due to the crystal symmetry, α-quartz has only two non-vanishing piezoelectric strain coefficients:
$d_{11} = +2.3 \times 10^{-12}$ m/V and $d_{14} = -0.67 \times 10^{-12}$ m/V **[8.I.5]**.
The resulting relative displacements $\Delta l/l$ caused by the mechanical strain are known as the converse piezoelectric effect.

Table 8.I.2 Matrix for the converse piezoelectric effect of quartz.

$$\begin{pmatrix} x_x \\ y_y \\ z_z \\ y_z \\ z_x \\ x_y \end{pmatrix} = \begin{pmatrix} \Delta l_x / l_x \\ \Delta l_y / l_y \\ \Delta l_z / l_z \\ \Delta\varphi_y / l_z = \Delta\varphi_z / l_y \\ \Delta\varphi_x / l_z = \Delta\varphi_z / l_x \\ \Delta\varphi_x / l_y = \Delta\varphi_y / l_x \end{pmatrix} = \begin{pmatrix} d_{11} & 0 & 0 \\ -d_{11} & 0 & 0 \\ 0 & 0 & 0 \\ d_{14} & 0 & 0 \\ 0 & -d_{14} & 0 \\ 0 & -2d_{11} & 0 \end{pmatrix} \times \begin{pmatrix} E_x \\ E_y \\ E_z \end{pmatrix}$$

According to the matrix shown in **Table 8.I.2** an electric field produces extensional (x_x, y_y, z_z) and shear (y_z, z_x, x_y) strains in one or more of the crystal axes. The key aspect in this work was to find a quartz crystal cut with a well matched piezoelectrically excited eigenmode to achieve high deformations Δl or $\Delta\varphi$. From the matrix it can be seen that the electrodes of this crystal cut have to be choosen in such a way that the electric field is orientated in the same direction as the high piezoelectric strain coefficients ($-2\,d_{11}$).
The mode and cut of interest are the fundamental thickness-shear mode of an AT cut of quartz (designation, (YXl)-35.25°; cristallographic notation of axes in this paper, x, y', z'), described in detail by Yong *et al.* **[8.I.6]**. The resonance frequency f_r depends on the thickness t of the resonating plate with $f_r = N/t$ (N= 1660 kHz·mm) **[8.I.7]**. A plate with a thickness t = 125 μm will therefore vibrate at a resonance frequency f_r = 13.3 MHz. Using a novel suitable design with an additional pair of electrodes the bossed and grooved diaphragm can be driven in a bending mode, comparable with that described in ref. **[8.I.8]** Alternating electric fields applied across the thickness of the diaphragm and oppositely directed produce oppositely directed body shear strains, causing a specific fundamental flexural vibration mode in the kHz range. A schematic diagram of the piezoelectric excitation principle is shown in **Fig. 8.I.9**.

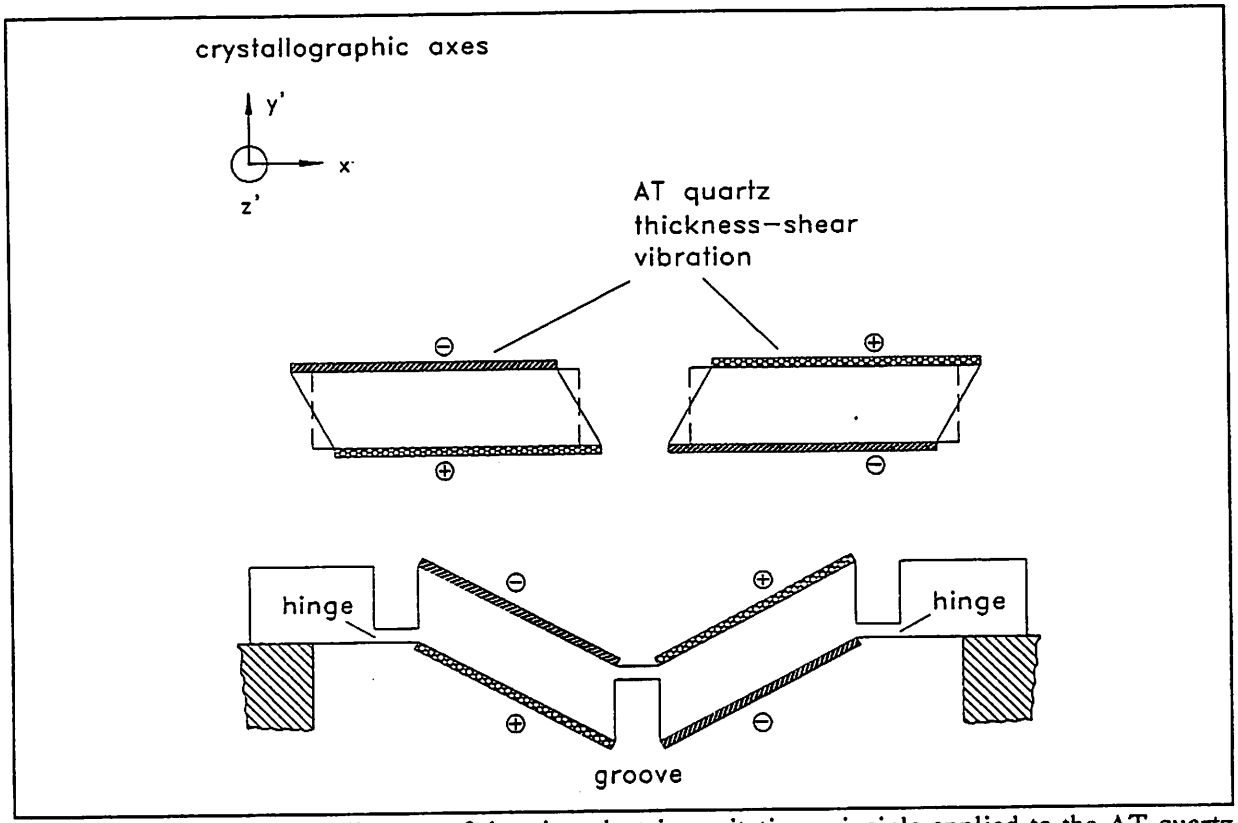

Fig. 8.I.9 Schematic diagram of the piezoelectric excitation principle applied to the AT-quartz diaphragms.

There are some other important advantages in using AT-quartz substrates, i.e., AT-quartz is a very commonly used low-cost material available in square 1.5 in blanks and has minimal temperature-dependent frequency shifts. For technological realization, full advantage can be taken of the high anisotropic etching rates of the AT-cut in HF solutions and the simple laser patterning of electrodes.

Design and simulation

The numerical finite element (FE) analysis method can be applied to predict sensor characteristics with reasonable accuracy and to analyze the effect of geometric modifications on the sensor performance. The FE software program ANSYS was used to predict the modal behaviour of the diaphragm. After geometric variations of the sensor shapes and dimensions, an optimized design was found comprising a diaphragm thickness t = 125 μm, a hinge width h_w = 50 μm, a hinge thickness h_t = 25 μm, and a diaphragm diameter d = 4200 μm, respectively (see **Fig. 8.I.10**). Using an axisymmetric FE-model with two-dimensional elements, a resonance frequency shift of 3.4 kHz for the fundamental mode f_o = 50 kHz relating to a pressure of 2.5 bar was calculated. An applied pressure of 2.5 bar causes a calculated material stress of 150 N/mm^2 at the hinge region, which is the maximal tolerable material stress for the diaphragms in this work. Using a FE model with three-dimensional elements for modelling the anisotropic material behavior, it can be shown that an increase of the diaphragm dimension in the z'- direction causes a higher electromechanical excitation efficiency, that is, a lower stiffness of the resonating diaphragm due to the piezoelectric strain coefficients (see **Table 8.I.2**). A schematic diagram of an oval-shaped diaphragm with its cross-sectional view is shown in **Fig. 8.I.10**.

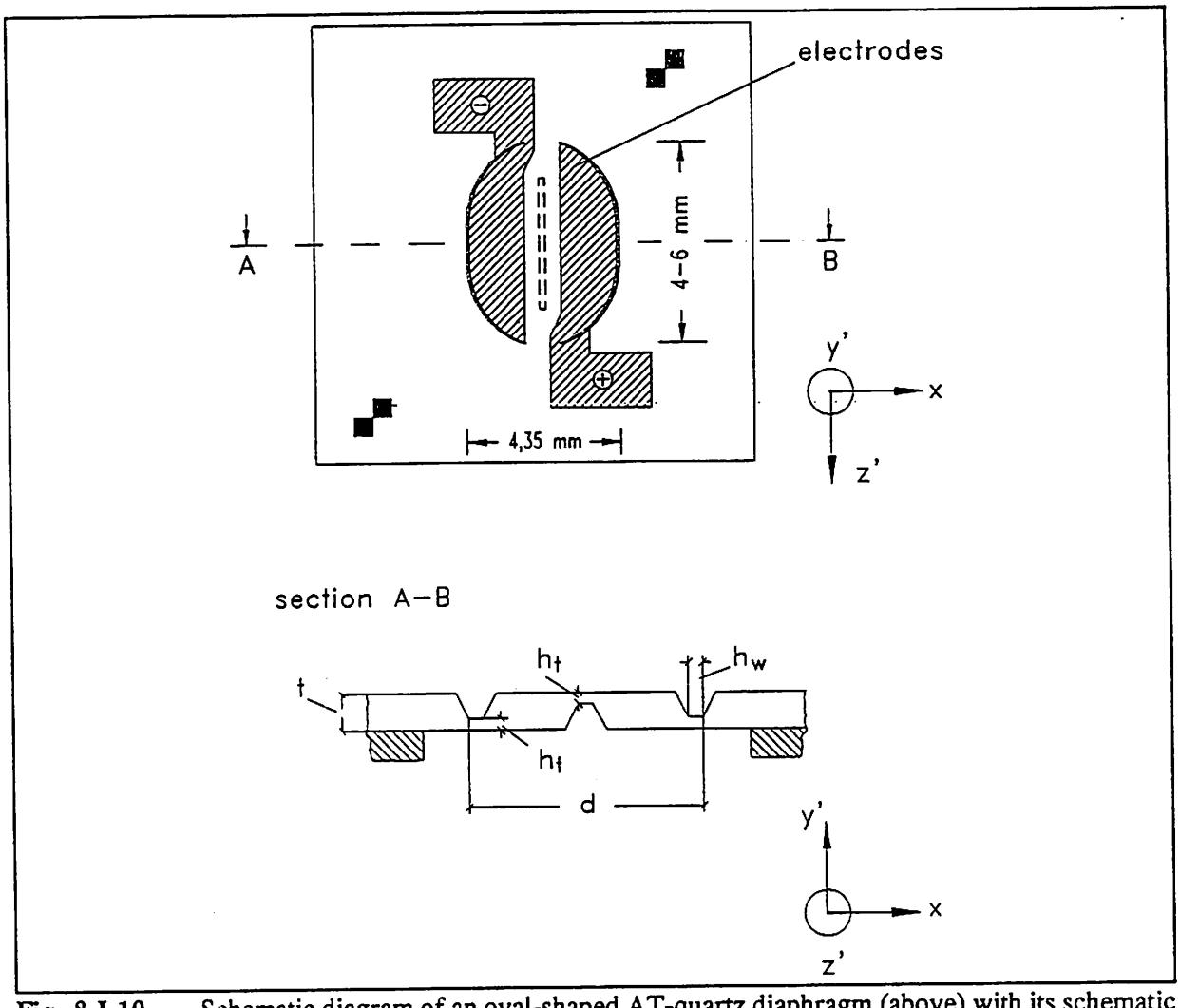

Fig. 8.I.10 Schematic diagram of an oval-shaped AT-quartz diaphragm (above) with its schematic cross-sectional view (below).

Technology

A low-cost batch fabrication process based on silicon micromachining equipment combined with a laser process to pattern the electrodes has been developed (see **Fig. 8.I.11**). After r.f. sputtering the Cr/Au metallization for etch-resistant and electrode layers, respectively, a photolithographic process is performed. A uniform layer of photoresist is deposited on both surfaces of the quartz blanks by a spin-on process. This process is well established in the IC manufacturing of circular silicon wafers. However, the square and very thin quartz blanks need to be processed simultaneously on both sides **[8.I.9]**. The resist drops thrown up at the corners of the blank make this processing step critical. A special chuck with an exactly dimensioned. square tub for quartz blanks and via-holes for vacuum application made of an anisotropically etched 3 in silicon wafer was developed for this purpose. Uniform layers of photoresist can be achieved with this chuck. After etching the Cr/Au layer, the quartz is chemically milled in an aqueous solution of ammonium fluoride and hydrofluoric acid at 80 °C . The etch rate was 1.3 μm/min and the etched depth was about 100 μm. The wet chemical etching behaviour of AT quartz is highly anisotropic **[8.I.2, 8.I.10]**. For compensating the underetching of concave and convex mask patterns on the lihographic mask layout, an etched ring-shaped test pattern with an inner radius of 2.9 mm and a width of 200 μm was evaluated.

The underetching of AT-cut quartz is schematically shown in **Fig. 8.I.13.**
The experimental etch rates are considered in a redesign of the lithographic mask layout to achieve a constant hinge width. With plasma processing techniques, quartz etching can be performed independently of the crystal structure with high etch rates **[8.I.11]**.
For this process step a plasma-etching technique can be a powerful but expensive alternative method. The next process step is the patterning of the Cr/Au metallization layer. A Nd:YAG laser system comprising a computer controlled x/y table was used to pattern the electrodes simultaneously on both sides of the quartz substrate. The width of the laser beam focus is 30 μm and the processing velocity is about 1 mm/sec.
The quartz diaphragm is mounted on a glass plate coated with a patterned conductive ITO (indium tin oxide) layer. An ultrasonic milled via-hole is drilled into the glass plate to apply pressure or vacuum to the sensor device. The quartz-to-glass mounting is performed by an UV adhesive filled with 22 μm thick ball spacers for overload protection. The electrical connections are made with conductive silver pads. After wire-bonding, the quartz/glass device is glued to an aluminum carrier.

Measurements and results

A laser vibrometer (POLYTEC OFV1102) was used to measure the mode spectra of the different quartz pressure sensors. The resonance frequency of a device under test excited by the synthesizer (sweep mode) of a spectrum-analyzer (Hewlett Packard HP3588A) in the fundamental bending mode is demonstrated in the amplitude/frequency characteristic of **Fig. 8.I.12.** The resonance peak of this sensor element was measured to about 36.2 kHz.
In principle the quartz sensor element can be mounted with either surfaces on the glass plate. The angle of the 'knee leverage' mentioned above will be closed or open, resulting in an increase or decrease of the resonance frequency, respectively. This can be demonstrated with the measured pressure-frequency characteristics of four different structured quartz sensor elements in **Fig. 8.I.14.** The excitation of the complete mounted sensor device is maintained in a two-port configured oscillator circuit comprising two amplification stages with symmetric difference amplification. Due to the capacitive coupling a low-pass phase shifter is used to suppress the common-mode signal.
The linearity error of the pressure-frequency signal response is shown in **Fig. 8.I.15.**
The maximum deviation in relation to the total frequency shift of the signal caused by an applied pressure change of 600 mbar is 1.8 %. The gauge factor g of a pressure sensor is defined as $g = (1/f_o) \cdot \Delta f / \Delta p$. For this sensor element the gauge factor amounts to g = 6.7% / bar, assuming a resonance frequency f_o = 35.4 kHz, a frequency change Δf = 1.4 kHz, and a pressure change Δp = 600 mbar.
The working range of the pressure sensors in this work is limited to 2 bar by the maximum material stress induced at the thin hinge regions of the quartz diaphragms.

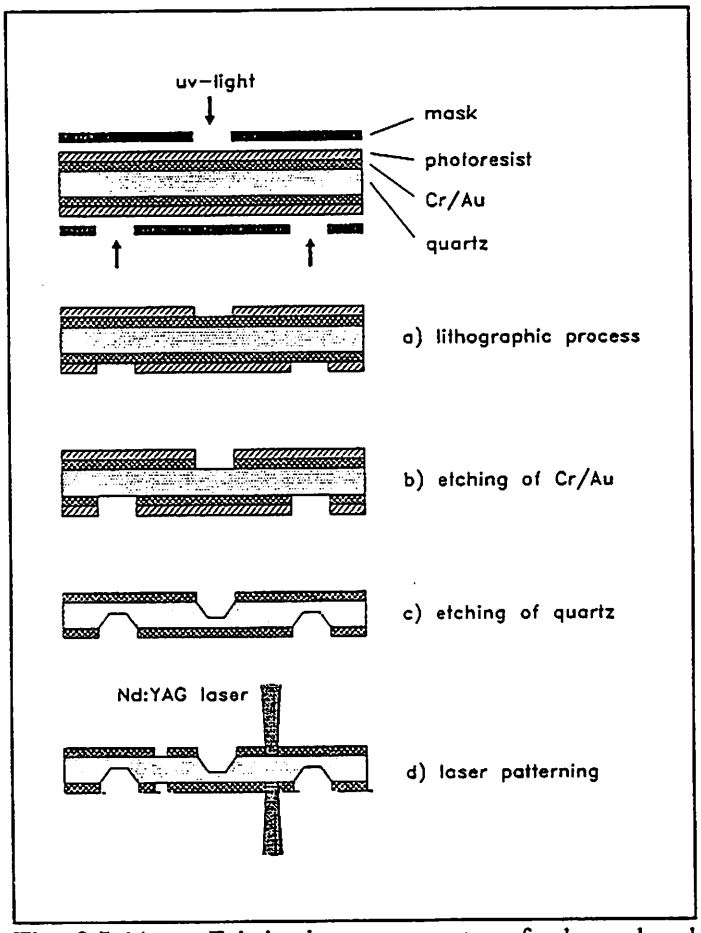

Fig. 8.I.11 Fabrication process steps for bossed and grooved AT-quartz diaphragms.

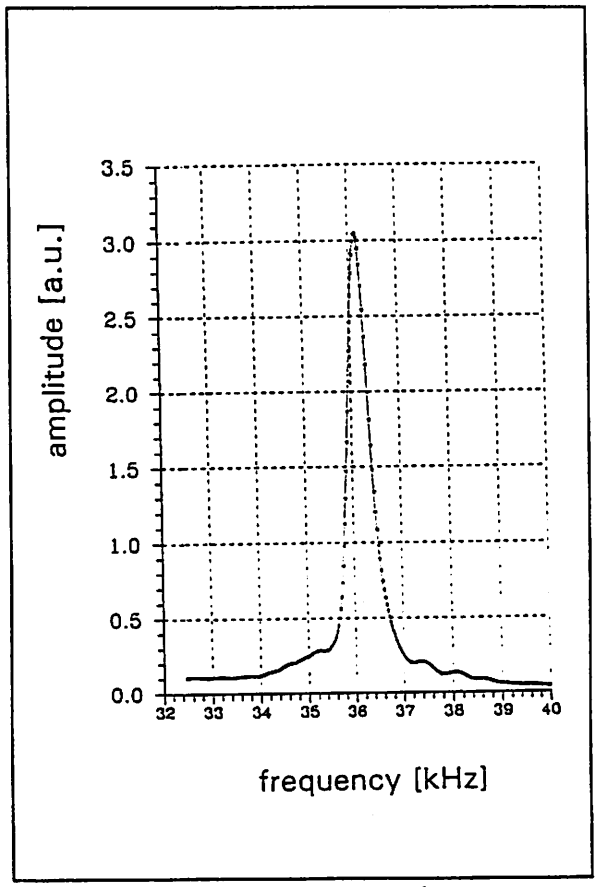

Fig. 8.I.12 Amplitude-frequency characteristic showing the fundamental bending mode of an AT-quartz diaphragm.

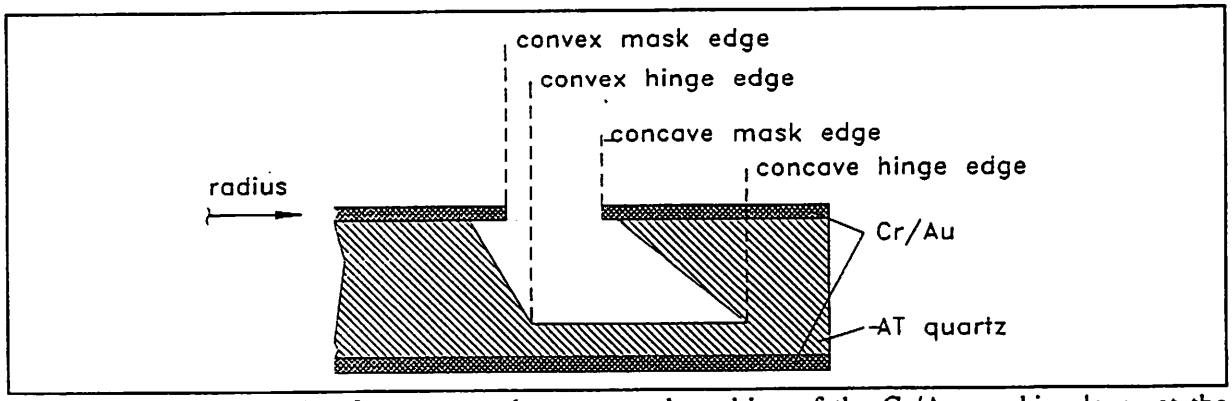

Fig. 8.I.13 Schematic of concave and convex underetching of the Cr/Au masking layer at the hinge region.

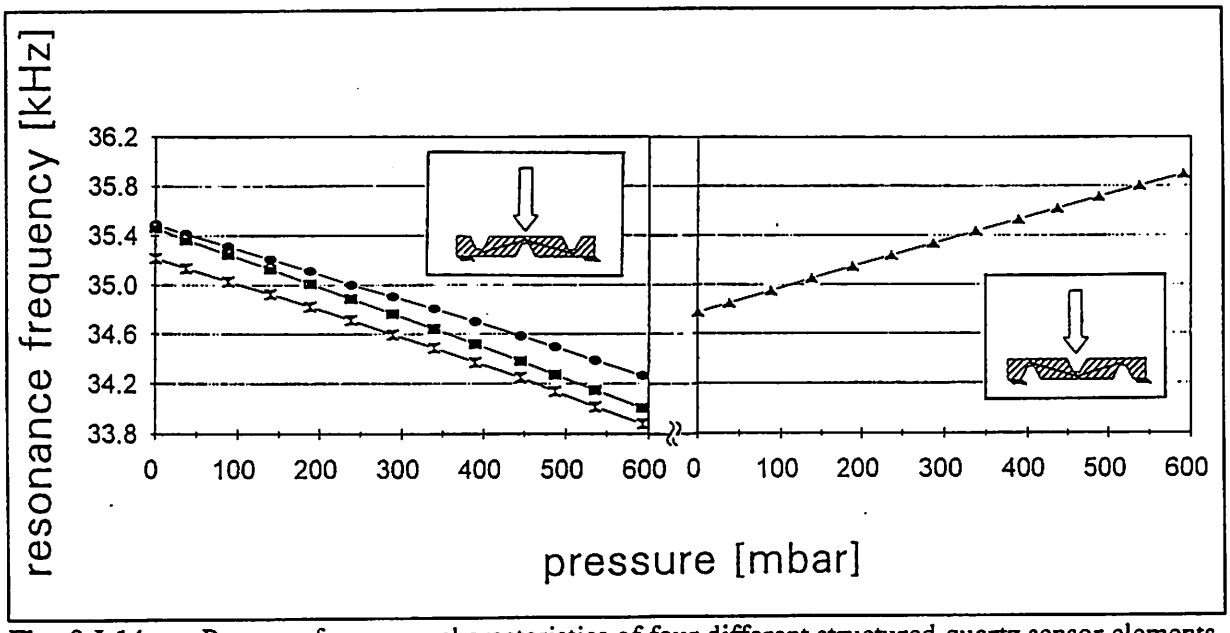

Fig. 8.I.14 Pressure-frequency characteristics of four different structured quartz sensor elements. Both kinds of mounting (i.e. quartz diaphragm with centre groove up or down) are possible, resulting in an increase or decrease of the resonance frequency caused by an applied external pressure load.

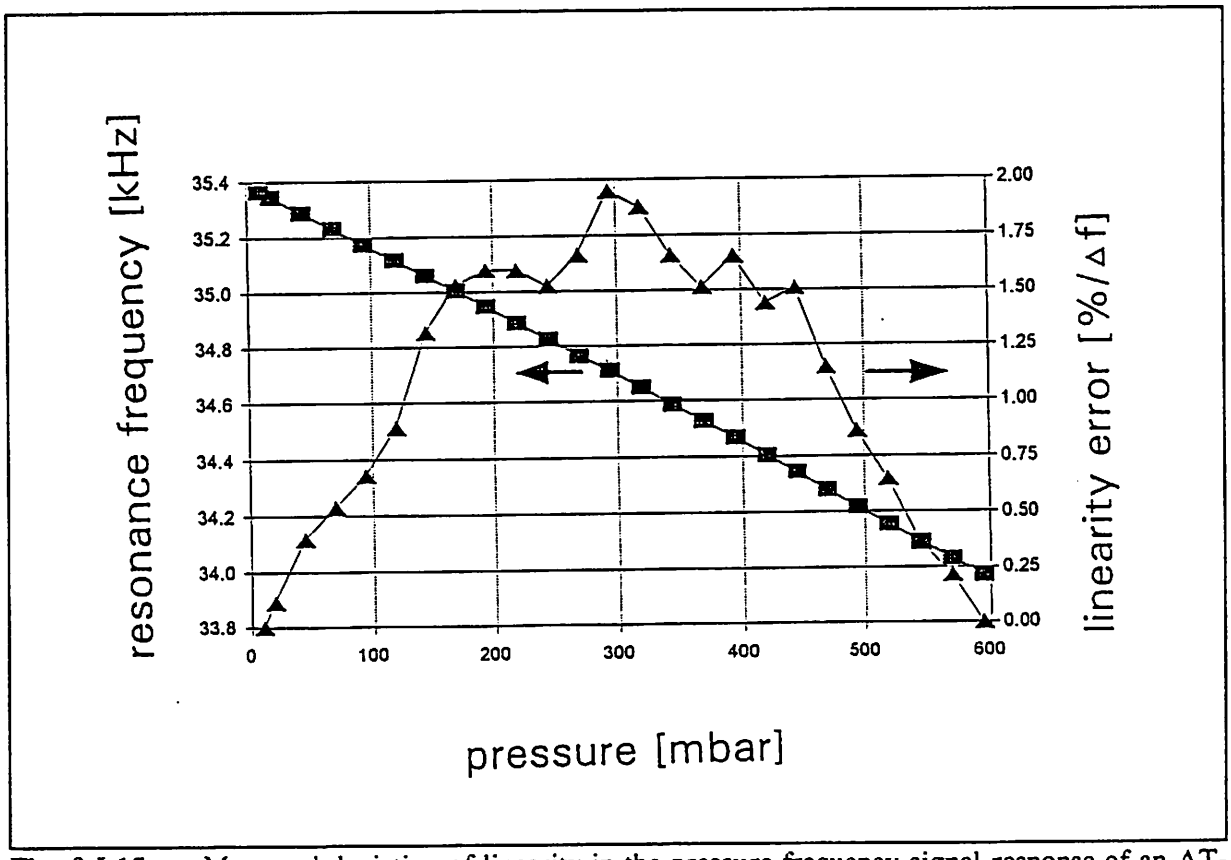

Fig. 8.I.15 Measured deviation of linearity in the pressure-frequency signal response of an AT-quartz pressure sensor (right). The hysteresis of the pressure-frequency characteristic cannot be resolved in this diagram.

8.I.4 Precision force transducers using mechanical resonators [8.I.28]

Force sensors can be built from miniaturized bulk devices if they are sensitive along one particular axis. For instance, it is possible to conceive a double-ended tuning-fork (DETF) resonator that is very sensitive to axial forces, such as in **Fig. 8.I.16** (see also **Fig. 7.1** in **Chapter 7**). This configuration is very interesting because of its excellent linearity, negligible hysteresis, good thermal stability, and low aging. Moreover, its sensitivity is very high: 10^{-3} / N between 0 - 10 N and a repeatability better than 6 x 10^{-4} over the force range.

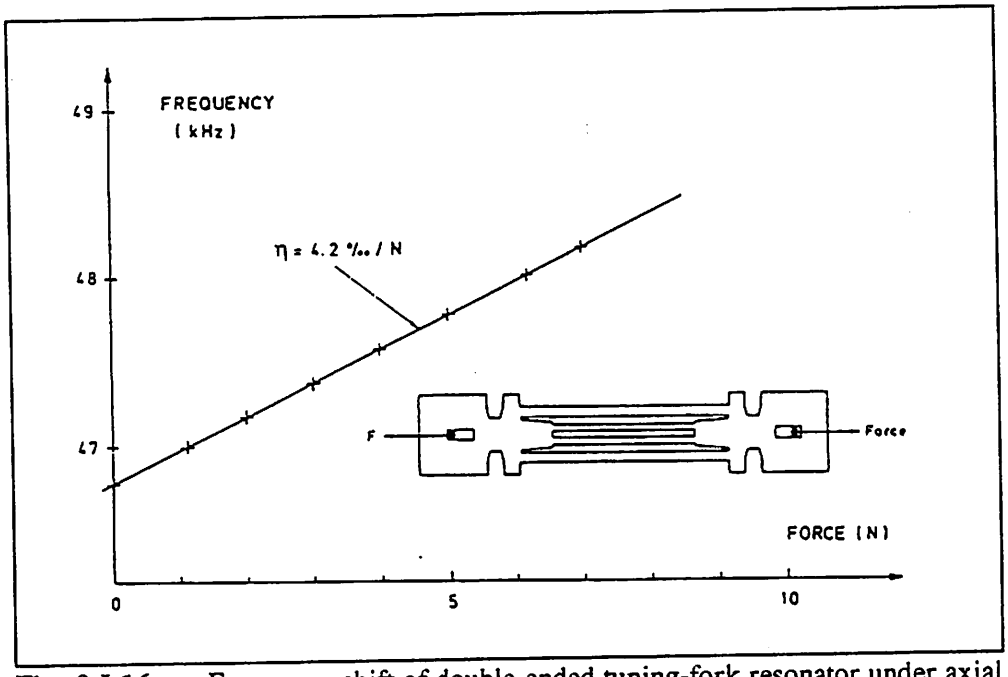

Fig. 8.I.16 Frequency shift of double-ended tuning-fork resonator under axial force [8.I.49].

Fig. 8.I.17 represents a construction of calibaration system for this force sensor [8.I.41]

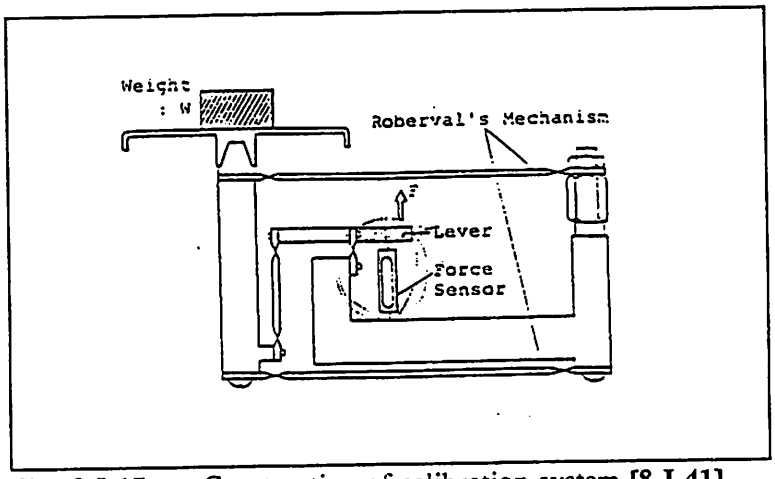

Fig. 8.I.17 Construction of calibration system [8.I.41].

The piezoelectric coupling for the quartz tuning fork in-plane flexure mode is schematically shown in **Fig. 8.I.18** [8.I.21].

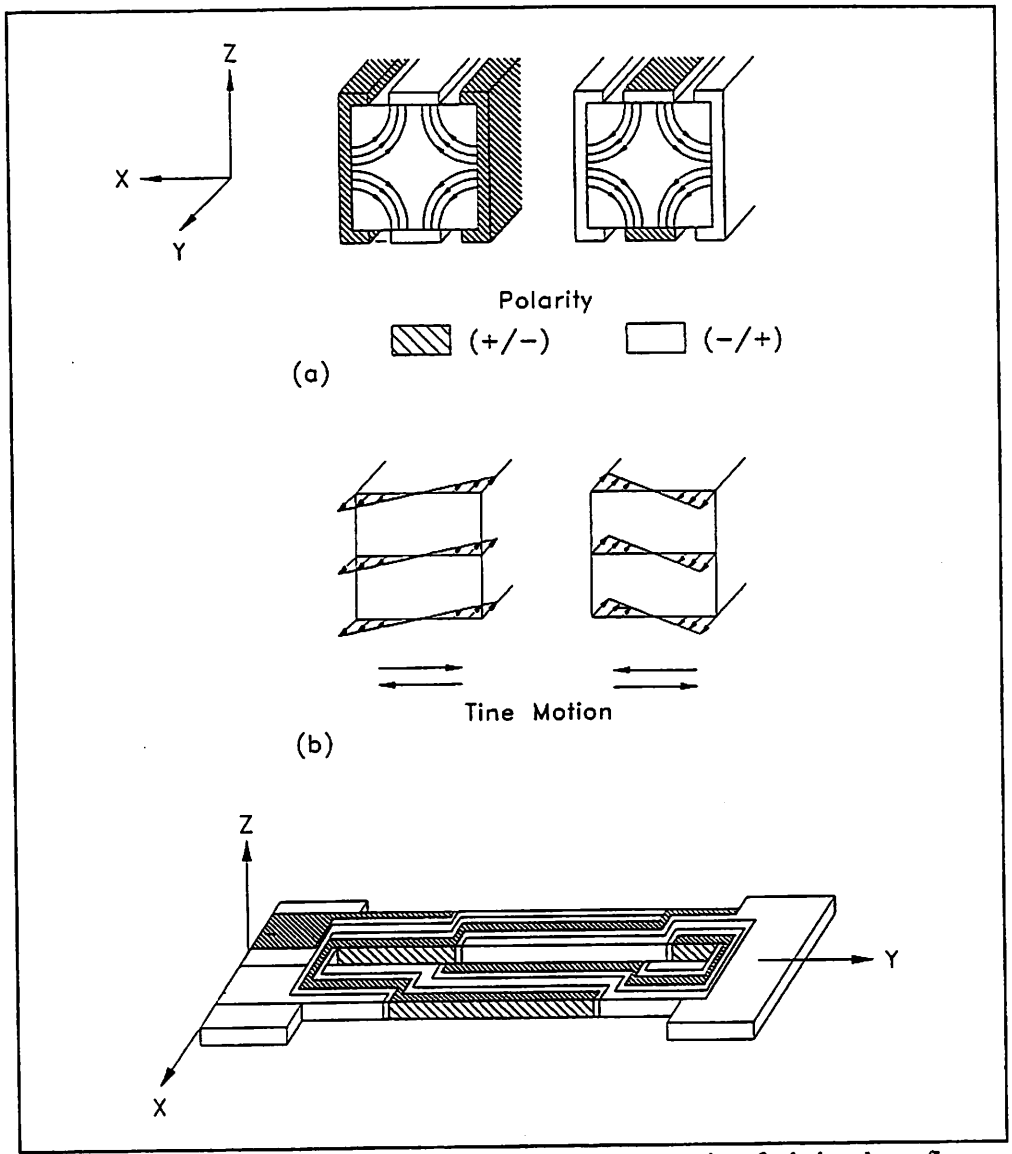

Fig. 8.I.18 Piezoelectric coupling for the quartz tuning fork in-plane flexure modes. (a) Flexure mode electric field distribution (E_x) tine cross-section. (b) Flexure mode induced stress distribution (σ_{yy}) tine cross-section. (c) DETF flexure mode electrode pattern.

8.I.5 Pressure sensor using quartz vibrating resonators [8.I.26]

Excitation

Using z-cut oriented wafers, only some of the components of the electric field oriented in the plane of the wafer are efficient. Therefore the electrodes of the piezoelectric capacitor must be as perpendicular as possible to the plane of the wafer (see also **Fig. 8.I.18**). This requirement can be met by micromachining a beam with steep vertical sides , and oriented along the so-called "mechanical" axis (ses **Fig. 8.I.5**). Electrodes evaporated on its sides allow an electric field to be generated along the "electrical" axis, creating a stress that sets the beam into vibration.

Most of the influence of the intrinsic parameters of the device may be strongly shadowed by the slightest defect in the way it is held or clamped, unless special decoupling has been designed. On the other hand, the advantage of decoupling may be cancelled out by the

appearance of undesirable modes of vibration, with frequencies close to that of the bridge, or in the span of its shift when a stress is applied. A compromise must be found to prevent the spreading of the resonator energy from reaching the outside of the sensor.

Aging

The long-term stability of quartz resonators has been shown to be good enough for most high-precision applications. Quartz resonators micromachined in z-oriented wafers with their axis along the y-direction show no long-term drift at room temperature, and, without any applied stress, an absolute thermal coefficient of frequency of resonance lower than 1 Hz / K.

Influence of a stress applied to the resonator

The basic idea is to convert a stress perpendicular to the wafer plane into a stress applied to the resonator lying in this plane.

The frequency shift of the resonator is caused by the applied stress adding a contribution (E_s) to the potential energy of the vibrating beam. If the stress applied to the beam is mostly localized in a small part of its volume, the yield strength may be reached for a low value of E_s, and hence of the frequency shift. That is why a uniform strain of the beam is a condition to get a higher frequency shift. A solution is proposed (**Fig. 8.I.19**) to stretch the vibrating beam without static flexion in order to prevent any inhomogeneous stress.

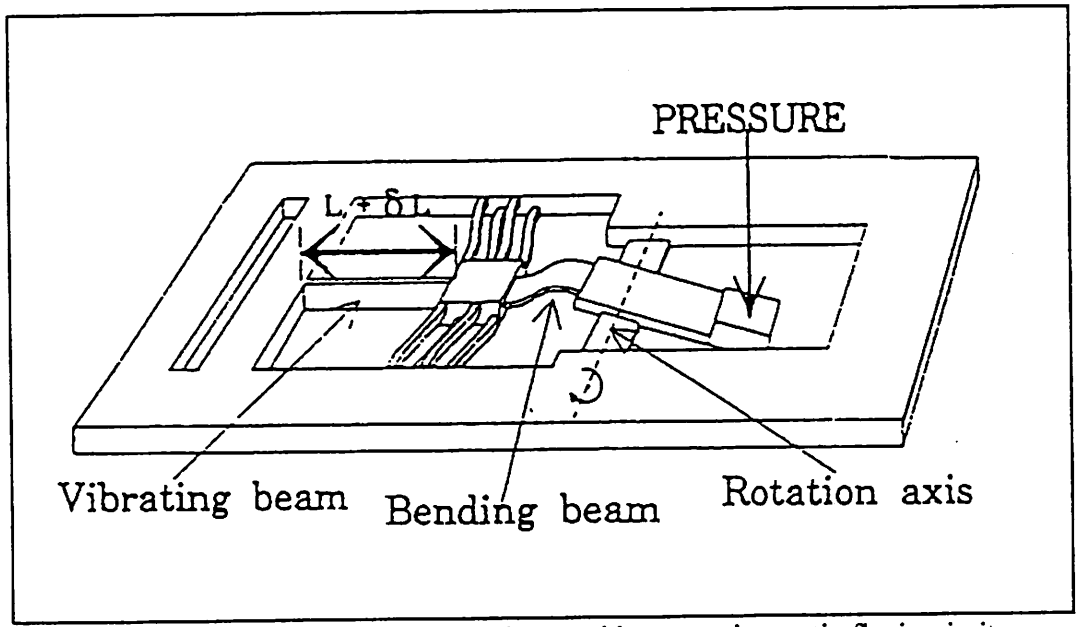

Fig. 8.I.19 Set-up for stretching the beam without causing static flexion in it.

Between the pivot and a bending structure where one end of the resonator is clamped, a bending beam is used to pull the bending structure and then the resonator itself. The bending beam and the bending structure are designed to cancel the static bending moment at the end of the resonator.

Fig. 8.I. 20 shows a prototype, chemically etched in a z-cut quartz wafer. The length of the resonator is 1.8 mm. **Fig. 8.I.21** shows the transfer function of one of these devices. The frequency span is here about 6 % of the unloaded resonance frequency. The complete device consists of three sealed wafers (**Fig. 8.I.22**). The middle wafer includes the resonator.

The upper wafer is mainly a membrane with a boss that pushes the extremity of the lever of the middle wafer. The lower wafer is used for hermetic sealing. The closure of the wafers is done by means of anodic bonding (see also **Fig. 8.I.8**).

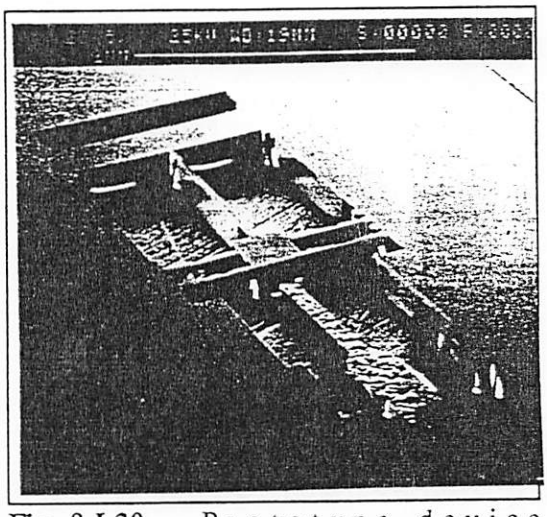

Fig. 8.I.20 Prototype device micromachined by chemical etching of a z-cut quartz.

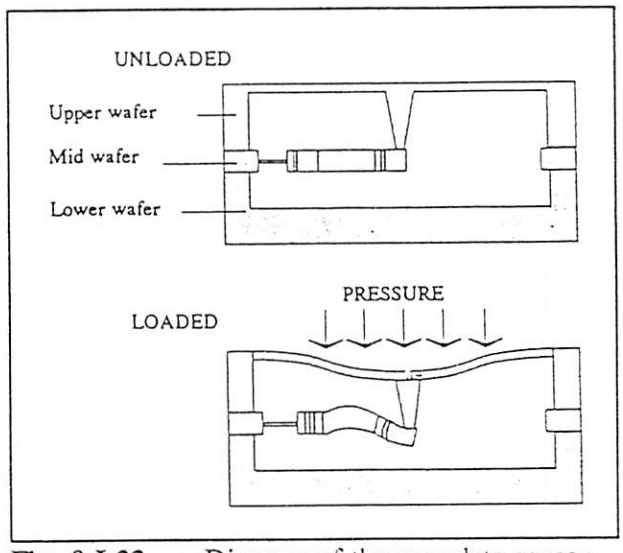

Fig. 8.I.22 Diagram of the complete sensor.

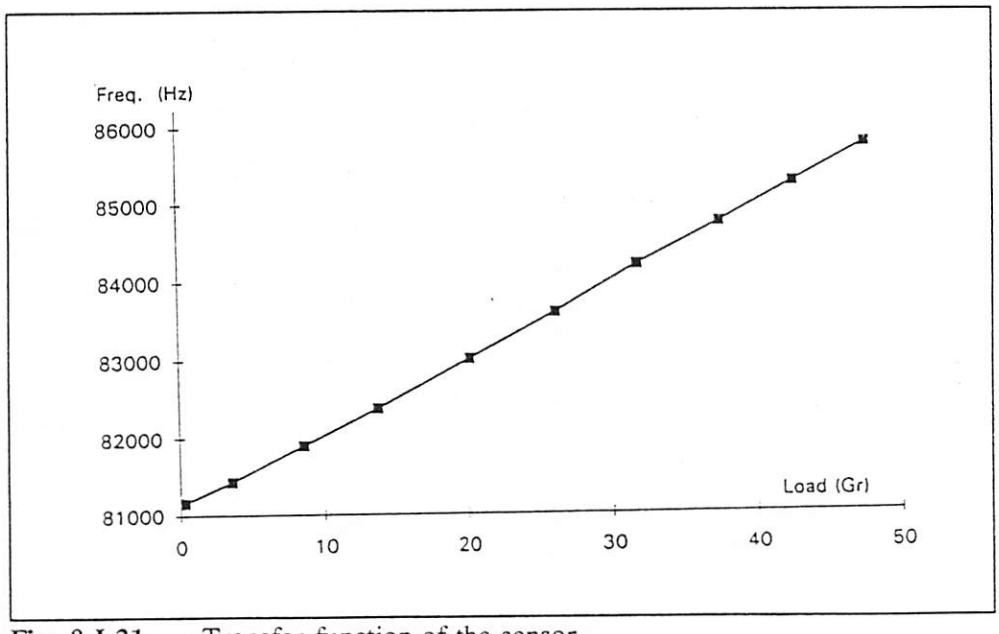

Fig. 8.I.21 Transfer function of the sensor.

8.I.6 The LETI-accelerometer [8.I.25]

Introduction

This sensor was developed in collaboration with SFENA. The whole mechanical part of the sensor is machined by anisotropic chemical etching of a z-cut quartz substrate. The etching speed is lower for the crystalline planes parallel to z-axes than for the other planes: thus it is possible to obtain right sides perpendicular to the substrate.

Operating principle

The accelerometer consists of a seismic mass, linked to the crystalline quartz wafer by two beams, flexible in the x-direction parallel to the wafer plane (see **Fig. 8.I.22**). A capacitive detector measures the mass displacement due to acceleration A_x. The surface of the mass is covered by a resistive foil, which allows the acceleration force $M \times A_x$ to be conteracted by a Laplace feedback force $I_y \times B_z$ when placed in a permanent magnetic field B_z and driving an electric current I.

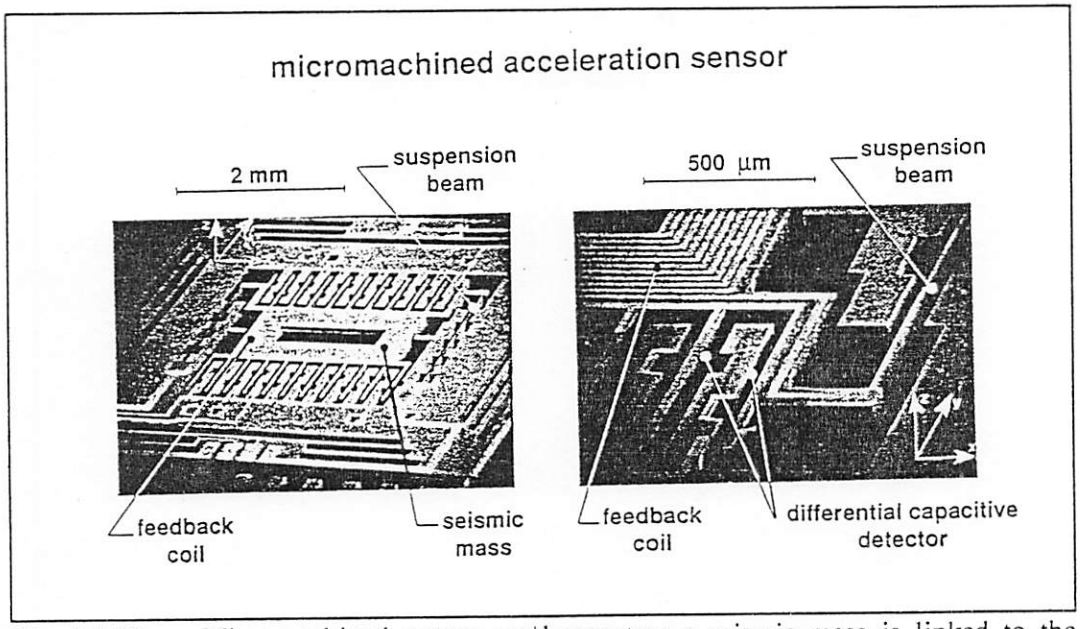

Fig. 8.I.22 Micromachined quartz accelerometer; a seismic mass is linked to the substrate by two beams flexible in the x direction; a capacitive detector measures the mass displacement due to acceleration A_x; a Laplace force $I_y \times B_z$ conteracts the acceleration force as a result of the coil) **[8.I.24]**.

Sensor characteristics of the complete accelerometer

- Range: $\pm$ 1 to $\pm$ 100 g
- Zero stability: $\pm$ 0,01 g
- Shock resistance: 20.000 g - 5 ms
- Quadratic non linearity: $< 20 \times 10^{-6}$ g/g^2
- Bandwidth: 50 Hz
- Mass: $<$ 10 g

References Chapter 8.I*

[8.I.1] S. Middelhoek, P.J. French, J.H. Huijsing and W.J. Lian, Sensors with digital or frequency output, *Sensors and Actuators, 15* (1988) 119-133.

[8.I.2] J.S. Danel, F. Michel and G. Delapierre, Micromachining of quartz and its application to an acceleration sensor, *Sensors and Actuators A21-A23* (1990) 971-977.

[8.I.3] US Patent No. 4 644 804, Febr. 24, 1987.

[8.I.4] R.H. Johnson, S. Karbassi, U. Sridhar and B. Speldrich, A high-sensitivity ribbed and bossed pressure transducer, *Sensors and Actuators A, 35* (1992) 93-99.

[8.I.5] R.W. Ward, The constants of alpha quartz, *Proc. 38th Annual Frequency Control Symposium, Philadelphia, PA, U.S.A., May 29 - June 1, 1984, pp. 22-31.*

[8.I.6] Y.-K. Yong and J.T. Stewart, Mass-frequency influence surface, mode shapes, and frequency spectrum of a rectangular AT-cut quartz plate, *IEEE Transactions on Ultrasonics, Ferroelectrics, and Frequency Control, Vol. 38, No. 1* (1991) 67-73.

[8.I.7] J.R. Hunt and R.C. Smythe, Chemically milled VHF and UHF AT-cut resonators, *Proc. 39th Annual Frequency Control Symposium, Philadelphia, PA, U.S.A., May 29-31, 1985, pp. 292-300.*

[8.I.8] US Patent No. 3 479 536, Nov. 18, 1969.

[8.I.9] B. Studer and W. Zingg, Technology and characteristics of chemically milled miniature quartz crystals, *Proc. 4th European Frequency and Time Forum, Neuchâtel, Switzerland, March 13-15, 1990, pp. 653-658.*

[8.I.10] J.S. Danel and G. Delapierre, Anisotropic crystal etching: a simulation programm, *Sensors and Actuators A, 31* (1992) 267-274.

[8.I.11] S. Schreiter and H.-U. Poll, A new plasma-etching technique for micromechanical structuring of quartz, *Sensors and Actuators A, 35* (1992) 137-141.

[8.I.12] H.-J. Wagner, W. Hartig and S. Büttgenbach, Design and fabrication of resonating AT-quartz diaphragms as pressure transducers, *Sensors and Actuators A, 41-42* (1994) 389-393.

* Oral presentation is based on further references:

[8.I.13] W.C. Albert, Force sensing using quartz crystal flexure resonators, *Proc. 38th Annual Frequency Control Symposium, 1984, pp. 233-239.*

[8.I.14] W.C. Albert, A low cost force sensing crystal resonator applied to weighing, *Proc. 42nd Annual Frequency Control Symposium, 1988, pp. 78-84.*

[8.I.15] ANSI/IEEE Standard 176-1978, Standard on piezoelectricity, *Transactions on Sonics and Ultrasonics, Vol. 31, No. 2* (1984) 1-55.

[8.I.16] Asulab S.A., *Capteur de force à résonateur à quartz*, Rapport condensé, 1985.

[8.I.17] R.J. Besson, New trends in quartz resonators developments and applications, *3. Congrès Européen de Chronométrie (CEC '90), Stuttgart, BRD, 25.-27. Oktober 1990, S. 173.*

[8.I.18] J.C. Brice, Crystals for quartz resonators, *Rev. Modern Physics, Vol. 57, No. 1* (1985) 105-146.

[8.I.19] S. Büttgenbach, Mikromechanische Quarzsensoren, *Fachbeilage Mikroperipherik in: Hard and Soft, No. 12* (1986) S. IV.

[8.I.20] S. Büttgenbach, Frequenzanaloge Quarzsensoren, *Fachbeilage Mikroperipherik in: Hard and Soft, No. 10* (1988) S. VI.

[8.I.21] L.D. Clayton, E.P. Eernisse, R.W. Ward and R.B. Wiggins, Miniature crystalline quartz electromechanical structures, *Sensors and Actuators, 20* (1989) 171-177.

[8.I.22] M. Christen und W. Hottinger, Schwingquarze als Sensoren, *Tagungsband AMA-Seminar Mikromechanik, 1989, pp. 209-223.*

[8.I.23] S.S. Chuang, Force sensor using double-ended tuning fork quartz crystals, *Proc. 37th Annual Frequency Control Symposium, 1983, p. 248.*

[8.I.24] J.S. Danel and G. Delapierre, Quartz: a material for microdevices, *J. Micromech. Microeng., 1* (1991) 187-198.

[8.I.25] G. Delapierre, J.S. Danel, F. Michel, J.L. Bost, A. Boura and O. Aujay, A quartz micromachined closed loop accelerometer, *Proc. 3rd Eurosensors 87, Cambridge, U.K., Sept. 22-24, 1987, pp. 223-224.*

[8.I.26] M. Dufour, M.T. Delaye, F. Michel, J.S. Danel, B. Diem and G. Delapierre, A comparison between micromachined pressure sensors using quartz or silicon vibrating beams, *Sensors and Actuators A, 34* (1992) 201-209.

[8.I.27] E.P. Eernisse, R.W. Ward and R.B. Wiggins, Survey of quartz bulk resonator sensor technologies, *IEEE Transactions on Utrasonics, Ferroelectrics, and Frequency Control, Vol. 35, No. 3* (1988) 323-330.

[8.I.28] D. Hauden, Miniaturized bulk and surface acoustic wave quartz oscillators used as sensors, *IEEE Transactions on Ultrasonics, Ferroelectrics, and Frequency Control, Vol. 34, No. 2* (1987) 253-258.

[8.I.29] C. Hedlund, U. Lindberg, U. Bucht and J. Söderkvist, Anisotropic etching of Z-cut quartz, *J. Micromech. Microeng., 3* (1993) 65-73.

[8.I.30] W.J. Kass and G.S. Snow, Double-ended tuning fork quartz accelerometer, *Proc. 40th Annual Frequency Control Symposium, 1986, pp. 230-236.*

[8.I.31] R.G. Kirman, A vibrating quartz force sensor, *Transducer Tempcon, Conference Papers, London, GB, June 14-16, 1983, pp. 98-121.*

[8.I.32] A. Kourepenis, A. Petrovich and M. Weinberg, Low cost quartz resonant accelerometer for aircraft inertial navigation, *Proc. 6th Int. Conf. Solid-State Sens. and Actuat., (Transducers'91), San Francisco, U.S.A., June 23-27, 1991, pp. 551-553.*

[8.I.33] K. Oguchi, E. Momosaki, +5°X micro quartz resonator by lithographic process, *Proc. 32nd Annual Frequency Control Symposium , 1978, pp. 277-281.*

[8.I.34] J. Söderkvist, design of a solid-state gyroscopic sensor made of quartz, *Sensors and Actuators, A21-A23* (1990) 293-296.

[8.I.35] J. Söderkvist, Piezoelectric beams and vibrating angular rate sensors, *IEEE Transactions on Ultrasonics, Ferroelectrics, and Frequency Control, Vol. 38, No. 3* (1991) 271-280.

[8.I.36] J. Söderkvist, Activation and detection of mechanical vibrations in piezoelectric beams, *Sensors and Actuators A, 32* (1992) 567-571.

[8.I.37] J. Söderkvist, Micromachined Gyroscopes, *Proc. 7th Int. Conf. Solid-State Sensors and Actuators (Transducers '93), Yokohama, Japan, June 7-10, 1993, pp. 638-641.*

[8.I.38] J.H. Staudte, Subminiature quartz tuning fork resonator, *Proc. 27th Annual Frequency Control Symposium, 1973, p. 50.*

[8.I.39] P. Suda, A.E. Zumsteg and W. Zingg, Anisotropy of etching rate for quartz in ammonium bifluoride, *Proc. 33rd Annual Symposium on Frequency Control, 1979, pp. 359-363.*

[8.I.40] H. Toshiyoshi, H. Fujita, T. Kawai and T. Ueda, A piezoelectrically operated optical chopper by quartz micromachining, *Proc. 7th Int. Conf. Solid-State Sensors and Actuators (Transducers '93), Yokohama, Japan, June 7-10, 1993, pp. 128-131*

[8.I.41] T. Ueda, F. Kohsaka and E. Ogita, Precision force transducers using mechanical resonators, *Proc. 10th Conf. on Measurement of Force and Mass, Kobe, Japan, Sept. 1984, pp. 17-22.*

[8.I.42] T. Ueda, F. Kohsaka, D. Yamazaki and T. Iino, Quartz crystal micromechanical devices, *Proc. 3rd Int. Conf. Solid-State Sensors and Actuators (Transducers '85), Philadelphia, PA, U.S.A., 1985, pp. 113-116.*

[8.I.43] T. Ueda, F. Kohsaka, T. Iino and D. Yamazaki, Temperature sensor using quartz tuning fork resonator, *Proc. 40th Annual Frequency Control Symposium, 1986, pp. 224-229.*

[8.I.44] T. Ueda, F. Kohsaka, T. Iino and D. Yamazaki, Theory to predict etching shapes in quartz crystal and its application to design devices, *Trans. Soc. Instr. Control Eng., Vol. 23, No. 12* (1987) 1-6.

[8.I.45] J.K. Vondeling, Fluoride-based etchants for quartz, *Journ. of Materials Science, 18* (1983) 304-314.

[8.I.46] R.D. Watkins, C.D. Tuthill, R.M. Curlee, D.R. Koehler and C.F. Joerg, Field assisted bonding of single crystal quartz, *Proc. 11th Quartz Dev. Conf. and Exhib., Kansas City, KS, U.S.A., Aug. 29-31, 1989, Vol. 1, pp. 6-17.*

[8.I.47] H.J. Wilhelmy, Mann und Werk: Jürgen Staudte und die Quarzstimmgabel, *Elektronik, No. 1* (1979) 38-42.

[8.I.48] R.B. Wiggins and E.P. Eernisse, Quarz tuning fork resonator transducers, *Private Communication Note / Preprint, 1986.*

[8.I.49] W. Zingg, Miniatur-Quarzschwinger und -Quarzsensoren, *Jahrbuch der Deutschen Gesellschaft für Chronometrie, Vol. 36, 1985, pp. 27-43.*

[8.I.50] D. Ang, Design and implementation of an etch system for production use, *Proc. 32nd Annual Symposium on Frequency Control, 1978, pp. 282-285.*

[8.I.51] G. Delapierre, Micro-machining: a survey of the most commonly used processes, *Sensors and Actuators, 17* (1989) 123-138.